J. Fluid Mech. (2013), *vol.* 722, *pp.* 645–664.
doi:10.1017/jfm.2013.145

Self-similar coalescence of clean foams

Peter S. Stewart[1,†] **and Stephen H. Davis**[2]

[1]Oxford Centre for Collaborative Applied Mathematics, Mathematical Institute, The University of Oxford, Oxford OX1 3LB, UK

[2]Department of Engineering Sciences and Applied Mathematics, McCormick School of Engineering and Applied Science, Northwestern University, Evanston, IL 60208, USA

(Received 1 April 2011; revised 28 November 2012; accepted 2 March 2013)

We consider the stability of a planar gas–liquid foam with low liquid fraction, in the absence of surfactants and stabilizing particles. We adopt a network modelling approach introduced by Stewart & Davis (*J. Rheol.*, vol. 56, 2012, p. 543), treating the gas bubbles as polygons, the accumulation of liquid at the bubble vertices (Plateau borders) as dynamic nodes and the liquid bridges separating the bubbles as uniformly thinning free films; these films can rupture due to van der Waals intermolecular attractions. The system is initialized as a periodic array of equally pressurized bubbles, with the initial film thicknesses sampled from a normal distribution. After an initial transient, the first film rupture initiates a phase of dynamic rearrangement where the bubbles rapidly coalesce, evolving toward a new quasi-equilibrium. We present Monte Carlo simulations of this coalescence process, examining the time intervals over which large-scale rearrangement occurs as a function of the model parameters. In addition, we show that when this time interval is rescaled appropriately, the evolution of the normalized number of bubbles is approximately self-similar.

Key words: complex fluids, foams, interfacial flows (free surface)

1. Introduction

Porous metallic solids can be manufactured to be strong yet exceedingly lightweight, making them useful materials in many engineering applications. Batch processing techniques for manufacturing such materials proceed by the rapid solidification of the corresponding gas–liquid foam (Banhart 2001). However, there are no available surfactants for molten metals and so these protocols typically insert particles (for example, SiC for molten Al) to reduce the rate at which the foam breaks up, or coarsens, in the time before it can be solidified. In the absence of these particles the gas bubbles coalesce rapidly, with breakup typically observed on time scales of milliseconds in experiments (Garcia-Moreno *et al.* 2008).

To understand the dynamics of coalescence in molten metallic foams with low liquid fraction we formulated a network model, described by Stewart & Davis (2012) (hereafter referred to as SD), for planar molten metallic foams; this model takes advantage of observation that as the liquid fraction of the foam decreases, the liquid flow field can be decomposed into two distinct regions: uniformly thinning

† Email address for correspondence: peter.stewart@maths.ox.ac.uk

liquid lamellae separating the gas bubbles (L), which drain toward accumulations of liquid around the bubble vertices known as Plateau borders (PBs). The asymptotic decomposition for drainage flow in an individual lamella, constructed by Breward & Howell (2002) (and extended by Brush & Davis (2005)), can then be employed to produce reduced models for the hydrodynamics in each region. In addition, we employ a criterion for film rupture driven by van der Waals intermolecular attractions derived by Anderson, Brush & Davis (2010). In SD, we employed this network model to elucidate the rate of bubble coalescence when the gas–liquid foam is confined within a solid box, observing that coarsening of the foam occurs in a number of distinct phases, influenced heavily by interactions with the solid boundaries. This network model approach has many similarities to vertex models for aqueous foams in both two (Bolton & Weaire 1992; Weaire *et al.* 1992) and three dimensions (Okuzono & Kawasaki 1995).

Aqueous foams, where surfactant has adsorbed to the interfaces and substantially slowed thinning rate of the liquid bridges, exhibit coarsening (or disproportionation or Ostwald ripening) driven by gas diffusion processes when the foam is disordered (Weaire & Hutzler 1999), facilitated by the T1 process where two PBs coalesce and separate in a more energetically favourable configuration (so a PB can interchange neighbouring bubbles) and the T2 process where a bubble disappears when all of the gas diffuses out across its boundaries. In the absence of film rupture, coarsening driven by gas diffusion (in both two-dimensional and three-dimensional dry foams) results in the average bubble side length scaling with $t^{1/2}$ for $t \gg 1$ where t is time (which can be derived formally from von Neumann's law (Weaire & Hutzler 1999)). Instability and coalescence can also be triggered by external perturbations to an aqueous foam, such as heating to induce a sequence of film ruptures, which triggers rapid coalescence through film breakage (Burnett *et al.* 1995); this coalescence process is inhomogeneous, where the average length of a bubble side grows slowly as a function of the increasing average bubble area compared with a foam coarsening by gas diffusion (Burnett *et al.* 1995; Chae & Tabor 1997; Hamsy *et al.* 1999). In addition, Vandewalle *et al.* (2001) produced acoustic measurements of popping bubbles in a coarsening aqueous foam, showing that the foam evolves by a series of intermittent avalanches which follow a power law for long times. Experiments indicate that coarsening through gas diffusion (or Ostwald ripening) is not sufficiently fast to account for breakup of molten metallic foams (Banhart *et al.* 2001). In contrast, in clean foams coarsening proceeds by bubble coalescence, driven by film thinning over two distinct phases. In the first phase, film rupture triggers a cascade of rapid topological rearrangement, which proceeds until the remaining films sweep up sufficient liquid to partially stabilize their interfaces, and where the foam reaches a new quasi-equilibrium (SD). The second phase of coalescence then proceeds by isolated rupture events, which occur intermittently over much longer time scales (SD).

Coarsening by coalescence is observed in a large number of other systems involving gas and liquid phases, such as liquid droplets on a prewetted surface (Gratton & Witelski 2008, 2009) or capillary drops on a conduit network (van Lengerich, Vogel & Steen 2010).

In this paper we use the network modelling approach of SD to understand the coarsening dynamics of molten metallic foams in periodic domains (where there are no boundaries to interact with) and perform Monte Carlo simulations for foams initially composed of a large numbers of bubbles. In § 2 we briefly summarize the network model of SD and discuss the extension to a planar periodic domain. In § 3 we describe large-scale statistical simulations over a range of parameter values, examining

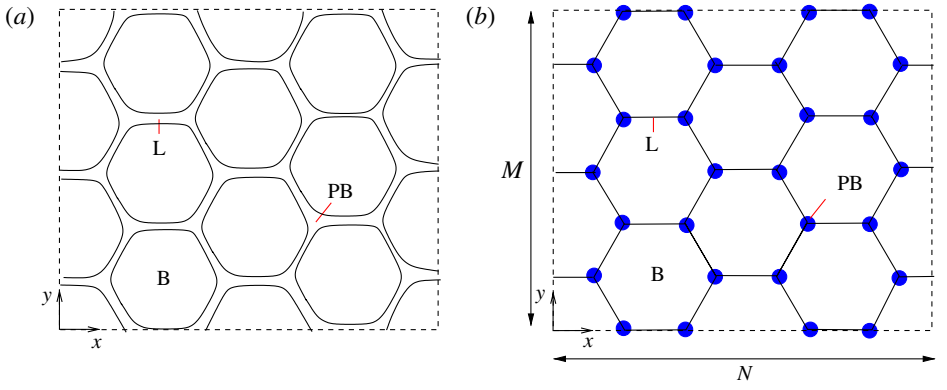

FIGURE 1. (Colour online) Schematic representation of a planar gas liquid foam with low liquid fraction, for $M = 3$, $N = 4$ in a two-dimensional periodic domain: (a) decomposition of the flow field into PBs and lamellae; (b) corresponding network of interconnected nodes and lines.

in particular the onset of coarsening and the rate of bubble coalescence. Finally, in § 4 we compare to coalescence simulations for a foam confined within a prewetted rigid box.

2. Summary of the network model

We consider the dynamics of a planar gas–liquid foam with constant liquid fraction ϕ; in general $0 < \phi \leqslant 1$, but here we restrict attention to low liquid fractions where $0 < \phi \lesssim 0.1$. The liquid phase is an incompressible Newtonian fluid of constant density ρ and viscosity μ, while the gas phase is assumed to be inviscid and compressible. We assume that both phases and the interfaces are clean (no particles or surfactants) and the temperature is held fixed everywhere; furthermore, the surface tension coefficient along each interface, γ, is assumed constant.

In SD we described a reduction of the full governing equations in the limit of low liquid fraction, starting from the Navier–Stokes equations for the liquid and an ideal gas law; the reduced system is composed only of ordinary differential equations and algebraic constraints, which forms a useful basis for conducting large-scale simulations with a much reduced computational cost compared with the full model. For the sake of brevity we do not repeat the derivation here, but simply highlight the key features of the modelling and present the resulting system of governing equations.

For low liquid fraction ϕ we decompose the flow field in a manner similar to models of dry aqueous foams (Weaire & Hutzler 1999): liquid accumulates in regions around the bubble vertices known as PBs; these borders are interconnected by very thin liquid films, known as lamellae, which form the edges of the bubbles. A typical foam composed of approximately regular hexagonal bubbles is shown in figure 1(a). Throughout this paper we restrict attention to foams initially composed of regular hexagonal bubbles of side length $2L$, arranged in a regular array ($M \times N$) confined within a rectangular periodic domain (illustrated in figure 1a). Other initial configurations and polydispersity can easily be considered within this modelling framework. In this paper we choose the periodic box so that one side is initially parallel to two of the bubble edges; this choice is not unique but the initial orientation of the foam within the box does not have any influence on the subsequent behaviour.

It should be noted that in this particular arrangement N must be even to ensure periodicity. We define coordinate axes parallel to the sides of the periodic box, denoted as $\hat{\boldsymbol{x}}$ and $\hat{\boldsymbol{y}}$, respectively, and describe position vectors as $\boldsymbol{x} = x\hat{\boldsymbol{x}} + y\hat{\boldsymbol{y}}$ (illustrated on figure 1*a*). To ensure that the rectangular periodic domain is compatible with the $M \times N$ array of bubbles we choose the side lengths of the box as $l_x = 3NL$ (along $\hat{\boldsymbol{x}}$) and $l_y = \sqrt{3}ML$ (along $\hat{\boldsymbol{y}}$), respectively. We further assume that the gas bubbles are all initially equally pressurized to $\hat{P}_0$, to ensure the initial array is a quasi-static equilibrium of the system (although the films will still be draining) and the nodes remain stationary until the system is perturbed by a film rupture. This is a great advantage in comparison to configurations in rectangular boxes (SD) where hexagonal bubbles cannot tessellate the domain perfectly and nodes must equilibrate over short time scales introducing a bias in the subsequent evolution.

The liquid fraction of the foam is assumed to be distributed equally among the $M \times N$ PBs (ignoring the small contribution in the thin lamellae, as is common in modelling dry foams), so the initial radius of curvature of each gas–liquid interface follows directly from the choice of liquid fraction ϕ,

$$\hat{a}_0 = L\left(\frac{3\sqrt{3}\phi}{\sqrt{3} - \dfrac{\pi}{2}}\right)^{1/2}. \tag{2.1}$$

We denote the typical thickness of a liquid film as $\hat{h}_0$, which we assume to be small compared with the length of the film, allowing a systematic reduction of the film dynamics to a one-dimensional system (Erneux & Davis 1993, § 2.2). This formulation results in the initial film thickness and the initial radius of curvature of the PB interfaces being independent.

We also incorporate the influence of van der Waals intermolecular attractions, which can drive instability on the film interfaces and subsequently rupture the film. The Hamaker constant describing the strength of these attractions between adjacent gas–liquid interfaces is denoted as $A^\star$.

In a similar manner to SD, we scale all lengths on L, velocities on the scale of lamellar drainage $U_0 = (\gamma/\mu)\,(\hat{h}_0/\hat{a}_0)^{1/2}$ (see Brush & Davis 2005), time on L/U_0 and pressures on the capillary scale γ/L. This results in six dimensionless groups

$$C = \frac{\mu U_0}{\gamma}, \quad R = \frac{\rho U_0 L}{\mu}, \quad S = \frac{A^\star}{6\pi\gamma L^2}, \quad h_0 = \frac{\hat{h}_0}{L}, \quad a_0 = \frac{\hat{a}_0}{L}, \quad P_0 = \frac{\hat{P}_0 L}{\gamma}, \tag{2.2}$$

the capillary, Reynolds and Sheludko numbers, the typical film aspect ratio and PB curvature and the initial bubble pressurization. Henceforth, all variables are dimensionless, unless otherwise stated.

The gas phase is assumed to be passive, so that the current bubble pressures P_j are spatially homogeneous and related to the area enclosed $A_{b,j}$ by an ideal gas law,

$$P_j A_{b,j} = P_0 A_0 \quad (j = 1, \ldots, MN), \tag{2.3}$$

where A_0 is the initial area of each bubble. As in SD, we ignore diffusion of gas between the bubbles. In aqueous foams the bubble pressure is typically much larger than the Young–Laplace pressure (γ/L). Here we investigate P_0 as a parameter in our model because the baseline pressurization in metallic foams will depend on the method used to produce the molten foam (e.g. blowing gas through a nozzle).

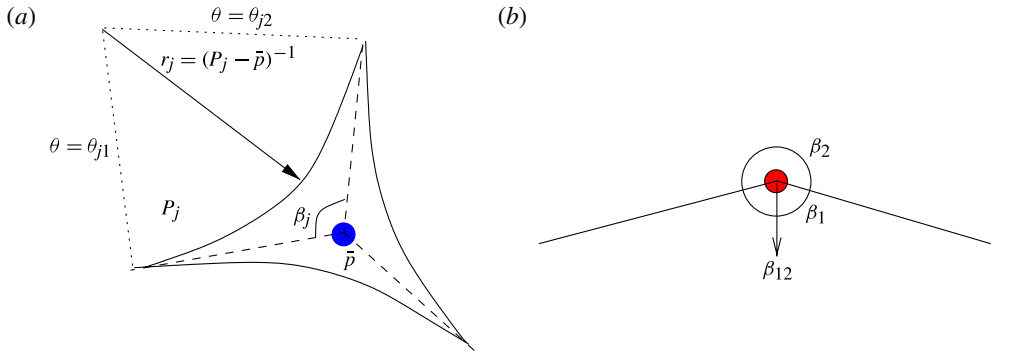

FIGURE 2. (Colour online) Schematic representation of a planar PB: (*a*) trijunction node; (*b*) redundant node.

In our network model reduction of the full equations (SD), we assume that all of the liquid in a PB acts through a single point, known as a node, which moves dynamically (§ 2.1); the lamellae map to lines along their midline (§ 2.2). The network analogue of the foam shown in figure 1(*a*) is shown in figure 1(*b*).

2.1. *Plateau borders to nodes*

The velocity scale U_0 has been chosen to ensure that $C = (h_0/a_0)^{1/2}$ (Breward & Howell 2002). We operate in the semi-arid limit, where $a_0 = O(1)$, $h_0 \ll 1$ (Brush & Davis 2005). Further assuming that the Reynolds number is $R = O(h_0^{1/2})$, the PB is capillary static at leading order with uniform pressure $\bar{p}$ and each compartment interface is an arc of constant curvature, meeting the midlines to the adjoining lamellae tangentially.

The total area of liquid in a PB in this outer model, where the surrounding films reduce to lines, takes the simple form

$$A_p = \sum_{j=1}^{3} (P_j - \bar{p})^{-2} \left\{ \tan\left[\frac{\pi}{2} - \frac{1}{2}\beta_j\right] - \frac{1}{2}(\pi - \beta_j) \right\} + O(C) \tag{2.4}$$

where β_j as the angle swept out between two neighbouring lamellae (figure 2*a*) and P_j is the gas pressure in the surrounding bubble.

Conservation of liquid area in the PBs takes the form,

$$\frac{\mathrm{d}A_p}{\mathrm{d}t} = \sum_{j=1}^{m} Q_j, \tag{2.5}$$

where the Q_m ($m = 2, 3$), the flux of liquid moving into/out of the PB, are constructed below. Once the area of liquid in the PB is known, the algebraic constraint (2.4) determines the liquid pressure $\bar{p}$.

For a conventional PB with three surrounding films, the total surface-tension force on interface j is proportional only to the angle swept out between the surrounding films, denoted $\theta_{j1} \leqslant \theta_j \leqslant \theta_{j2}$ (see figure 2*a*),

$$\boldsymbol{F}_j = \left[\hat{\boldsymbol{x}} \sin\theta - \hat{\boldsymbol{y}} \cos\theta\right]_{\theta_{j1}}^{\theta_{j2}} + O(C) \quad (j = 1, 2, 3). \tag{2.6}$$

However, when one of the three films surrounding a PB ruptures, that node becomes redundant and will equilibrate under surface tension, where the force is proportional to the difference in angle swept out on either side of the two surrounding films, denoted as β_1 and β_2, respectively (see the derivation in SD and figure 2*b*),

$$\boldsymbol{F}_j = (-1)^j \beta_j \hat{\boldsymbol{\beta}}_{12} + O(C) \quad (j = 1, 2), \tag{2.7}$$

where $\hat{\boldsymbol{\beta}}_{12}$ is a unit vector in the direction parallel to the line which originates at the node and bisects the angle β_1 (figure 2*b*)

Following SD, a force balance about the geometric centre of the PB leads to an evolution equation for the position $\boldsymbol{X}$ and speed $\boldsymbol{U}$ of the nodes in the form

$$\frac{\mathrm{d}\boldsymbol{X}}{\mathrm{d}t} = \boldsymbol{U}, \tag{2.8a}$$

$$RC\frac{\mathrm{d}}{\mathrm{d}t}(A_p\boldsymbol{U}) = \sum_{j=1}^{m} \boldsymbol{F}_j - C\boldsymbol{g}(\boldsymbol{U})A_p. \tag{2.8b}$$

The source of each term is discussed in detail in SD, but we pay special attention to the damping term with unknown functional $\boldsymbol{g}$; we follow SD in assuming that this is linearly proportional to the node speed, $\boldsymbol{g} = K\boldsymbol{U}$, similar to Kern *et al.* (2004), where K is a constant.

2.2. *Thinning lamellae*

The liquid lamellae bend to accommodate a pressure drop between the bubbles on either side and drain liquid into the surrounding PB interfaces due to capillary viscous suction. We assume bending is instantaneous to accommodate a pressure drop between two bubbles of pressures P_1 and P_2, so that the radius of curvature of the film midline is given by the Young–Laplace equation $r = 2/|P_1 - P_2|$ and the uniform liquid pressure p_0 is the average of the gas pressures on either side, $p_0 = (P_1 + P_2)/2$.

We approximate the length of the lamella by the straight-line distance between the two surrounding nodes, denoted as l. In SD, we highlighted two possible limits on how liquid area is exchanged between the PBs and the films as the nodes move. We termed these limits extrusion and elongation; in the former limit the film is extruded from the ends with constant thickness (so the area in the PB is changed) whereas in the latter the lamella will elongate or contract while conserving area. In SD, we allocated a parameter, λ, which spanned these two limits. We found slight differences between the foam evolution in these two limits at early times, but these were due mainly to the short time scale adjustment necessary for foams confined within a solid box; in this paper we focus on the elongation limit, but do not expect significant differences in these periodic domains, especially in the first phase of coalescence which is of interest below. From Brush & Davis (2005) the drainage rate of a film of uniform thickness h_L and length l can be written as

$$\frac{\mathrm{d}h_L}{\mathrm{d}t} = -\frac{h_L}{l}\frac{\mathrm{d}l}{\mathrm{d}t} - \sum_{i=1}^{2}\frac{Q_i}{l}. \tag{2.9}$$

The drainage flux from the film into a trijunction PB can be determined by matching through a transition region (Breward & Howell 2002), and is determined by the

pressure drop from the film

$$Q = \frac{3}{16}\left(\frac{2a_0(p_0 - \bar{p}_k)h_L^3}{h_0}\right)^{1/2}. \tag{2.10a}$$

When a node becomes redundant, the flow then reverses and moves into the two remaining films, at a rate we assume proportional to the current film thickness,

$$Q = -\hat{Q}h_L, \tag{2.10b}$$

where $\hat{Q}$ is a constant.

2.3. *Rupture criterion*

We omit van der Waals forces explicitly in the governing equations, but following Anderson *et al.* (2010) we employ a rupture criterion for the films, which states that van der Waals instabilities will begin to grow toward rupture when the instantaneous film thickness satisfies

$$h_L < \left(\frac{8\alpha S}{f\,(\bar{a}/\alpha)}\right) \tag{2.11}$$

where α is the ratio of the current film length to its initial length and f is a function computed numerically by Anderson *et al.* (2010) and incorporated directly into our model.

Once the film has broken, we instantly allow the two broken lamellar arms to retract into the surrounding PBs, which now become redundant, with only two surrounding films. These nodes then evolve according to (2.8*b*) with the surface tension force given by (2.7) and liquid drains into the surrounding films according to (2.10*b*). Once all of the liquid has drained out of these nodes, they are then removed from the calculation and the two surrounding films are merged into one new lamella.

2.4. *T1 and T2 transitions*

When any two nodes come within a distance $D \ll 1$ apart, we enforce a topological rearrangement, known as a T1 transition, where the two PBs merge and separate in a new configuration with a lower surface energy. Because we do account for surface energy here, this transition proceeds by a simple rearrangement of the nodes (see the schematic in figure 3), very similar to that in the vertex models described by Weaire & Hutzler (1999) and the new film is approximately orthogonal to the engulfed film. Full details of the numerical implementation are given in SD. However, in the simulations below we observe that T1 events are exceeding rare in these clean foams.

Because gas diffusion across the liquid films is ignored, T2 transitions, where all of the gas diffuses out of a bubble, cannot occur. This is consistent with the experimental observations of Banhart *et al.* (2001), where breakup of the foam is observed to occur on time scales much faster than Ostwald ripening.

2.5. *Numerical procedure*

A brief summary of the model structure is provided in table 1, listing the equations used to solve for each dependent variable. Numerical simulations of this model are conducted in MATLAB using the `ode15s` package. Topological changes to the system, such as film rupture, T1 transition and node deletion are detected using the `events` package. Absolute and relative error tolerances are chosen to ensure less than 0.1 %

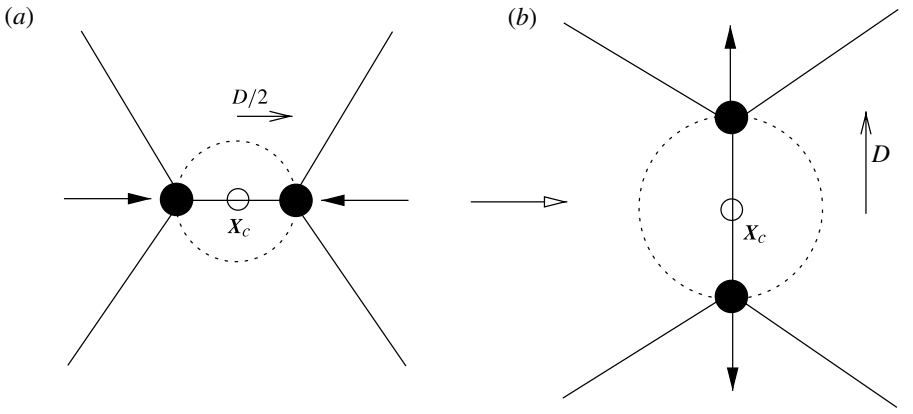

FIGURE 3. Schematic representation of a T1 transition, where the new film after merger is approximately perpendicular to the initial film.

Variable	Symbol	Equation	Initial number
Node position	$\boldsymbol{X}$	(2.8*a*)	$4NM$
Node speed	$\boldsymbol{U}$	(2.8*b*)	$4NM$
PB pressure	$\bar{p}$	(2.4)	$2NM$
PB liquid area	A_p	(2.5)	$2NM$
Lamella and film thickness	h_L	(2.9)	$3NM$
Bubble pressure	P	(2.3)	NM

TABLE 1. Summary of the network model, where the number of equations refers to the initial configuration for an NM array of equally sized hexagonal bubbles.

error in first rupture time. In addition, total liquid volume is conserved within 0.1 % over each simulation.

In this study we ignore the extra bubble area introduced by the bending of the lamellae. This can be easily included within our formulation and, indeed, was present in the simulations of SD. However, including this effect significantly increases the number of dependent variables in the system, as the bubble pressures cannot be immediately deduced from the bubble area. In this paper, our primary interest is in the first phase of coalescence, before the redundant nodes are absorbed into the surrounding films, so the bubble shape is well approximated by the polynomial portion of the bubble. This assumption will lead to significant errors when bubbles have less than three sides (see the examples in SD), but in the simulations below this occurs long after the first phase of coarsening has ended.

3. Foam coarsening in a periodic domain

To gain insight into the coarsening of the foam through film rupture and bubble coalescence, we conduct large-scale simulations of the network model described in § 2. We introduce stochastic effects by sampling the initial film thickness from a normal distribution with mean h_0 and standard deviation d,

$$h_L(0) = N(h_0, d^2 h_0^2). \tag{3.1}$$

We initialize the foam as a regular array of hexagonal bubbles, equally pressurized to P_0. In molten metallic foams the pressurization of the bubbles depends on the processing method, so we investigate the dependency on this parameter below.

As in SD, we set the Reynolds number $R = C = (h_0/a_0)^{1/2}$. The model then has four independent dimensionless parameters, the initial film thickness h_0, the foam liquid fraction ϕ, the Sheludko number S and the baseline pressure in the bubbles, P_0. In addition, we are interested in the dependency on the standard deviation in the initial film thicknesses, d. We also have two 'lumped' parameters for our model, which we set to $K = 10$ and $Q = 1$ throughout the simulations. As in SD, node motion is overdamped.

In particular, we consider foam geometries consisting of $M = 4$, $N = 8$ (32 bubbles), $M = 5$, $N = 10$ (50 bubbles), $M = 6$, $N = 12$ (72 bubbles), $M = 7$, $N = 14$ (98 bubbles) and $M = 8$, $N = 16$ (128 bubbles). In figure 4 we illustrate a benchmark example of coarsening in a foam initially consisting of 72 bubbles. The first rupture ($t = 21.632$) initiates a dramatic period of coarsening, with 57 ruptures occurring over a time interval of 0.7095 time units. In these panels solid lines represent lamellae, filled black circles represent trijunction nodes and open circles represent redundant nodes. A movie of the foam dynamics is provided as online supplementary material available at http://dx.doi.org/10.1017/jfm.2013.145. Furthermore, our model also allows us to trace the liquid pressure in the nodes and the total area of liquid in each PB (see SD for an example).

We measure the coalescence of the foam by examining the evolution of the total number of bubbles for each simulation, denoted as $\mathcal{N}_b(t)$, and shown in figure 5(a) corresponding to the stills shown in figure 4. It should be noted that this is a discrete measure; in SD we also examined the root mean square (r.m.s.) node speed as a continuous measure of coarsening through coalescence, but small discontinuities introduced by film rupture make this measure highly irregular (see figure 5b). The simulation saturates to a plateau number of bubbles, reaching a new quasi-equilibrium, which corresponds to the end of the first phase of coalescence. The remaining films have swept up large amounts of liquid from the redundant PBs and are thus partially stabilized. Further ruptures occur over much longer time scales, when these films have thinned sufficiently.

To account for the stochastic initial conditions we conduct a large number of simulations of the model (32 in this case), using initial conditions sampled according to (3.1), for each parameter combination of interest. Quantities denoted with an overbar represent an ensemble average over these simulations. We define the inter-rupture time, denoted δt, as the average time between subsequent ruptures over the time taken for the foam to evolve to half the initial number of bubbles. For our purposes, we define the first phase of coalescence as having ended when the gap between subsequent ruptures is greater than $10\overline{\delta t}$ time units. From each simulation we document the first rupture time, denoted t_R, the length of the first phase of coalescence, denoted Δt, and the change in the number bubbles over the first phase of coalescence, denoted $\Delta\mathcal{N}$. Also, since the velocity scale of lamellar drainage depends implicitly on the liquid fraction of the foam, we are also interested in the first rupture time, t_C, with respect to the capillary velocity scale $U_c = \gamma/\mu$. In table 2 we list the mean and standard deviation of these quantities over 32 runs for a variety of parameter combinations.

We begin by considering the onset of instability (§ 3.1), followed by an examination of the rate of coarsening, showing that the rescaled coarsening curves are approximately self-similar (§ 3.2).

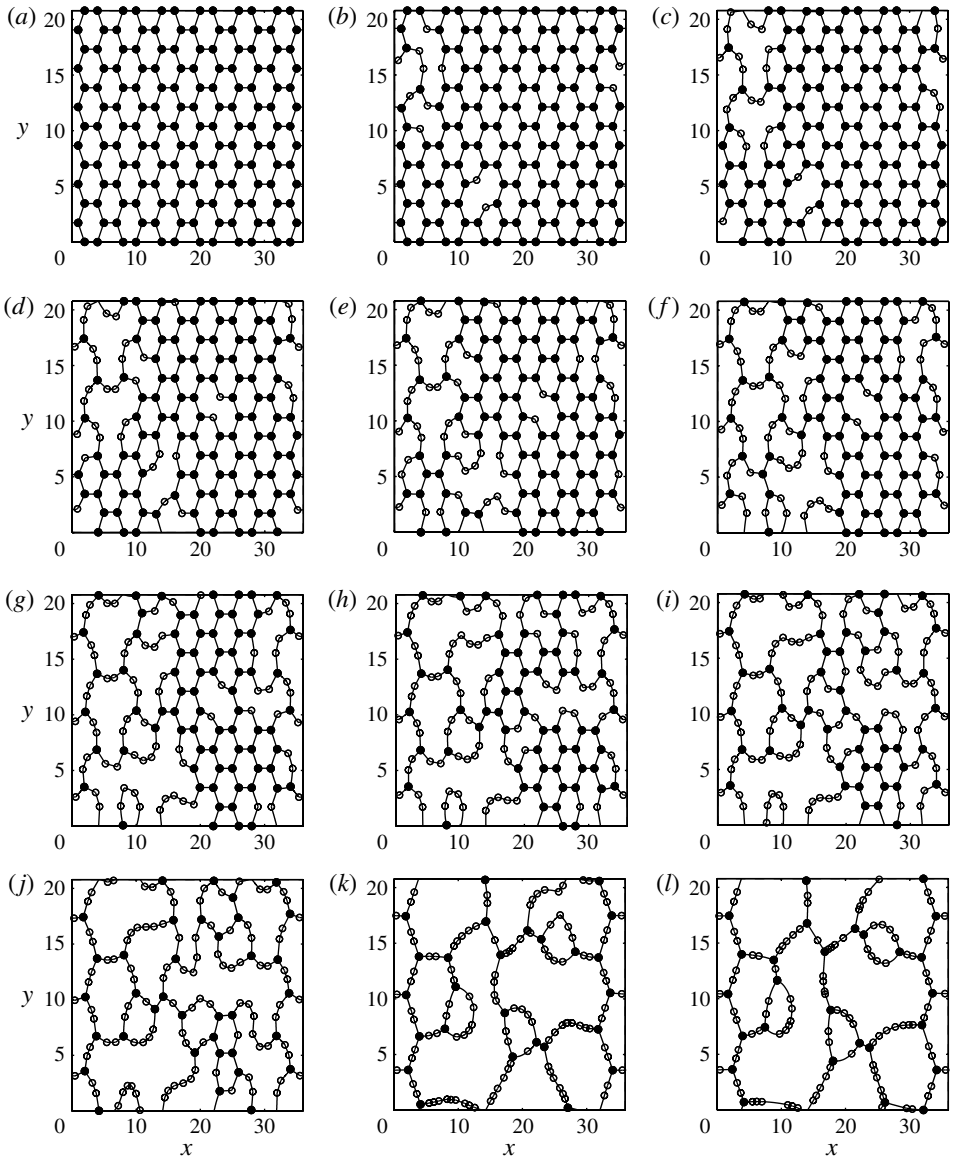

FIGURE 4. A typical example of foam coalescence in a foam initially composed of 72 bubbles: (*a–l*) 12 snapshots of the foam structure over the first phase of coalescence. Here, the parameters in the model are fixed as $P_0 = 1.0$, $S = 10^{-10}$, $\phi = 0.05$ and $h_0 = 0.01$: (*a*) $t = 21.6315$; (*b*) $t = 21.8779$; (*c*) $t = 21.9765$; (*d*) $t = 22.0241$; (*e*) $t = 22.0566$; (*f*) $t = 22.1069$; (*g*) $t = 22.1409$; (*h*) $t = 22.1854$; (*i*) $t = 22.2255$.

3.1. *The onset of bubble coalescence*

We initialize the foam as a regular array of equally pressurized bubbles. Until the first film breakage occurs, the foam is in static equilibrium and the bubble pressures remain constant (unlike in SD, where there was a period of short scale rearrangement due to confinement in a box) and the lamellae are essentially thinning independently; there is modest coupling between the thinning films as the liquid pressure in the nodes will

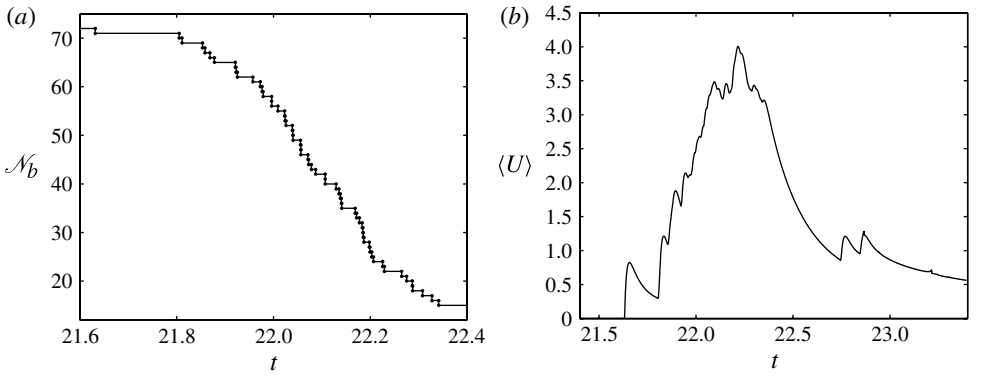

FIGURE 5. The stepwise coalescence of the foam, for the topological rearrangement shown in figure 4: (*a*) the evolution of the total number of bubbles; (*b*) the r.m.s. node speed.

increase slightly as liquid drains from the surrounding lamellae (see SD), but this will make only a small difference to the onset of rupture.

The instability criterion for a single foam lamella (2.11) (obtained by Anderson *et al.* (2010)), indicates that rupture is promoted by decreasing the initial film thickness or by increasing the Sheludko number of the flow. Also, as shown in table 2, the time until the first film rupture increases as the liquid fraction of the foam increases when measured on the capillary time scale. These deductions are consistent with observations in SD.

We observe that changing the initial baseline pressure in the bubble makes no appreciable change in the first rupture time (see table 2). This is to be expected, as when the foam is arranged as equally sized bubbles in static equilibrium (figure 4*a*), the system is dependent on the pressure drop between the films and the PBs which drives the drainage flow, but independent of the absolute value of the baseline pressure.

However, increasing the variability in the initial film thickness serves to reduce the first rupture time significantly and, hence, promote coarsening by coalescence (see table 2). This is also to be expected, as when the foam is regularly arranged the first film to rupture is that which is assigned the least initial thickness, and on average the minimum film thickness assigned will decrease as the variability in the initial condition increases.

3.2. *The rate of bubble coalescence*

To examine the rate at which the bubbles coalesce for a variety of initial foam sizes, we first normalize the current number of bubbles by the initial number for that arrangement $\mathcal{N} = \mathcal{N}_b/\mathcal{N}_b(0)$, so that $0 \leqslant \mathcal{N} \leqslant 1$.

As a first method for comparing the data, we superimpose the plot of the current number of bubbles against time for 32 runs of the model for four initial foam sizes: $\mathcal{N}_b(0) = 50, 72, 98, 128$ shown in figure 6(*a*), holding the system parameters fixed: $P_0 = 1$, $S = 10^{-10}$, $\phi = 0.05$, where an overbar represents an ensemble average over these simulations (summary statistics for these runs are listed in table 2). These curves trace out the change in the normalized number of bubbles over time and are similar in shape, but since the first rupture time varies over an interval the rate of coalescence

https://doi.org/10.1017/jfm.2013.145 Published online by Cambridge University Press

M	N	h_0	d	ϕ	S	P_0	$\bar{t}_R$	$\bar{t}_C$	$\overline{\Delta\mathscr{N}}$	$\overline{\Delta t}$	$\overline{\delta t}$
4	8	0.01	0.1	0.05	10^{-10}	1.0	21.8932 (±0.22713)	246.656 (±2.559)	25.5938 (±1.8467)	0.66856 (±0.22118)	0.025129
5	50	0.01	0.1	0.05	10^{-10}	1.0	21.8166 (±0.21778)	245.7924 (±2.4535)	41.125 (±2.0635)	0.79649 (±0.19638)	0.019042
6	12	0.01	0.1	0.05	10^{-10}	1.0	21.7311 (±0.18995)	244.829 (±2.140)	59.250 (±2.3827)	0.84224 (±0.18498)	0.014489
6	12	0.01	0.1	0.05	10^{-10}	10.0	21.633 (±0.30504)	243.4963 (±3.4334)	56.5625 (±3.1309)	0.69027 (±0.18003)	0.011522
6	12	0.01	0.1	0.05	10^{-10}	50.0	21.7724 (±0.25317)	245.066 (±2.8496)	56.6875 (±3.3929)	0.55997 (±0.1405)	0.0091631
6	12	0.01	0.05	0.05	10^{-10}	1.0	22.5706 (±0.094768)	254.288 (±1.0677)	59.6562 (±2.5604)	0.43978 (±0.091679)	0.007325
6	12	0.01	0.2	0.05	10^{-10}	1.0	19.1588 (±0.7675)	215.8493 (±8.6469)	60.9375 (±2.5265)	2.7453 (±0.73856)	0.049276
6	12	0.01	0.1	0.025	10^{-10}	1.0	22.5384 (±0.2746)	213.5255 (±2.6015)	58.8125 (±3.0101)	0.62203 (±0.14989)	0.010538
6	12	0.01	0.1	0.01	10^{-10}	1.0	23.8257 (±0.36289)	179.5168 (±2.7342)	59.0 (±3.0161)	0.53254 (±0.1268)	0.0089961
7	14	0.01	0.1	0.05	10^{-10}	1.0	21.4847 (±0.25858)	242.0532 (±2.9132)	80.25 (±3.3118)	1.0571 (±0.23135)	0.013286
8	16	0.01	0.1	0.05	10^{-10}	1.0	21.4973 (±0.310)	242.1957 (±3.4925)	104.875 (±3.2204)	1.0418 (±0.30259)	0.010412
8	11	0.01	0.1	0.07832	10^{-10}	1.0	18.9245 (±0.26034)	213.2098 (±2.9311)	58.0625 (±2.271)	2.883 (±0.45143)	0.051943

TABLE 2. Summary of Monte Carlo simulations of the network model. Quantities denoted in brackets represent one standard deviation from the mean over 32 simulations.

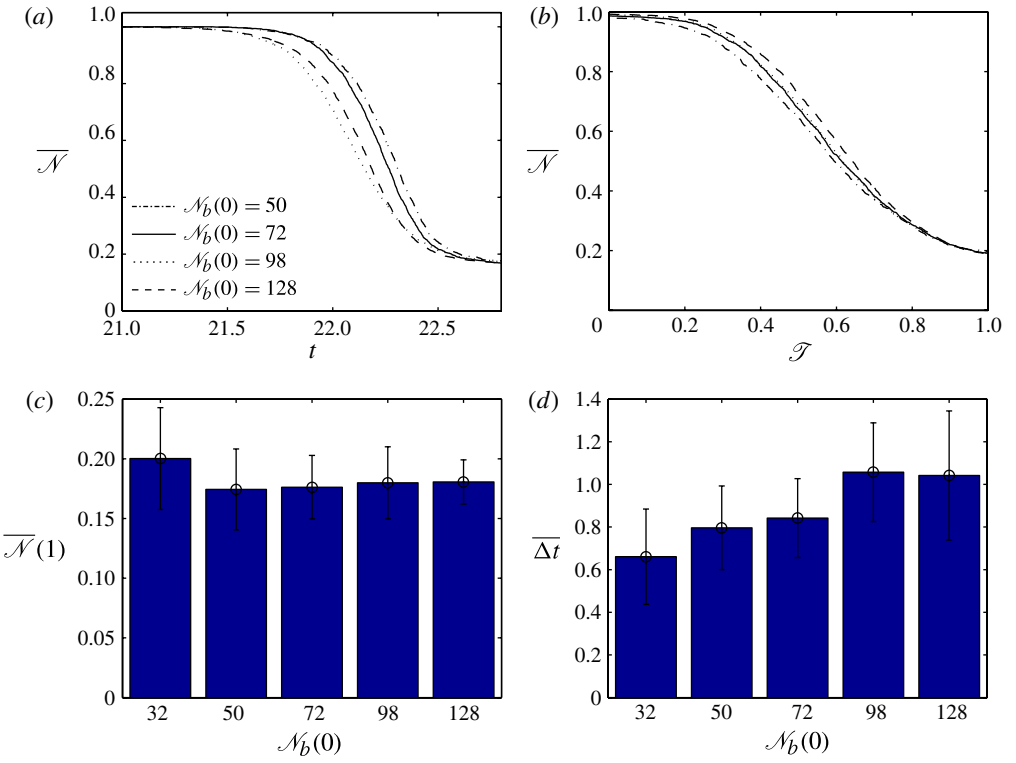

FIGURE 6. (Colour online) The dependency on the initial size of the foam: (*a*) the evolution of the normalized number of bubbles over time, t; (*b*) the evolution of the normalized number of bubbles over rescaled time $\mathscr{T}$; (*c*) histogram of the normalized number of bubbles at the end of the first phase of coarsening; (*d*) histogram of the time interval for the first phase of coarsening. Here, the other parameters in the model are fixed as $P_0 = 1.0$, $S = 10^{-10}$, $\phi = 0.05$ and $h_0 = 0.01$.

estimated from the superimposed data is not an accurate reflection of the individual simulations.

A more meaningful method for comparing the data is to rescale time according to

$$\mathscr{T} = \frac{t - t_R}{\Delta t} \quad (t \geqslant t_R), \tag{3.2}$$

so that $0 \leqslant \mathscr{T} \leqslant 1$ and the length of the phase of coalescence becomes unity in this new measure. Replotting the averaged number of bubbles against this rescaled time is shown in figure 6(*b*). Because time is now normalized with respect to the first rupture time, the normalized number of bubbles at $\mathscr{T} = 0$ is a small amount less than one, $\mathscr{N}(0) = (\mathscr{N}_b(0) - 1)/\mathscr{N}_b(0) < 1$. However, $\mathscr{N}(0) \to 1$ as $\mathscr{N}_b(0) \to \infty$, so this effect becomes less important as the initial number of bubbles increases. Figure 6(*b*) suggests that these curves are now approximately self-similar. Another indication of self-similarity is that normalized number of bubbles in the foam at the end of the first phase of coarsening is approximately constant (see the histogram in figure 6*c*), between 17 and 20 % of the initial number. However, the time interval over which this coalescence occurs increases with the initial number of bubbles, but appears to saturate as the $\mathscr{N}_b(0)$ becomes large (figure 6*d*), so the normalized coarsening

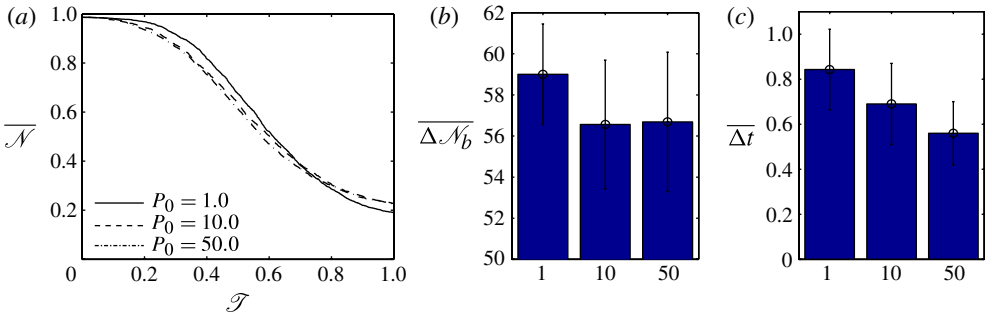

FIGURE 7. (Colour online) The role of baseline bubble pressurization in a foam initially composed of 72 bubbles, for 3 particular choices $P_0 = 1.0$, $P_0 = 10.0$ and $P_0 = 50.0$: (*a*) the change in the normalized number of bubbles against rescaled time; (*b*) histogram of the number of ruptures in the first phase of coalescence; (*c*) histogram of the time interval for the first phase of coalescence. Here, the other system parameters are fixed as $\phi = 0.05$, $h_0 = 0.01$, $S = 10^{-10}$ and $d = 0.1$.

curves become approximately independent of the initial number of bubbles. However, it would require a larger number of simulations in larger foams to conclude this self-similarity definitively.

3.3. *Baseline bubble pressurization*

Foams can be produced by a variety of techniques, which will result in different baseline pressure in the bubbles, so we investigate the rate of bubble coalescence as a function of this parameter. Time is once again normalized according to (3.2), where the corresponding change in the number of bubbles is shown in figure 7(*a*) for $P_0 = 1.0$, $P_0 = 10.0$ and $P_0 = 50.0$ holding all other parameters fixed. Interestingly, we again observe that the evolution of the normalized number of bubbles is approximately self-similar and the mean number of bubbles remaining in the system after the large-scale rearrangement is approximately constant (figure 7*b*). This is in contrast to observations in SD, where we found that the number of ruptures in the first phase was strongly dependent on the baseline bubble pressure, but we attribute this effect to confinement within the rigid box. However, the baseline bubble pressure has a dramatic effect on the time taken for this first phase of coalescence, with the mean time taken for the first phase decreasing as P_0 increases (figure 7*c*).

3.4. *Foam liquid fraction*

The liquid fraction of the foam remains constant throughout the simulations; initially the bulk of the liquid is located within the PBs, but as coalescence progresses the liquid gradually accumulates in the remaining films, which then stabilizes them to further ruptures. We investigate the rate of coalescence as a function of the foam liquid fraction, examining the change in the number of bubbles against time (rescaled according to (3.2)), where the curves again appear to be approximately self-similar (figure 8*a,b*), with the time interval for the first phase of coalescence decreasing as the liquid fraction decreases (figure 8*c*). This trend is also evident when the comparisons are made on the capillary time scale.

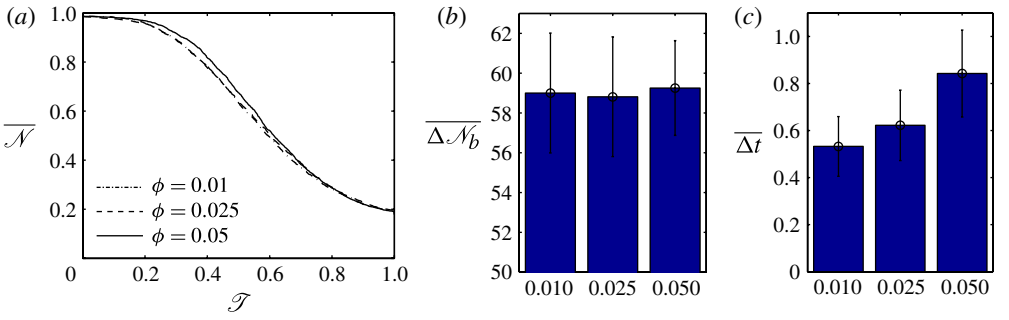

FIGURE 8. (Colour online) The role of liquid fraction in a foam initially composed of 72 bubbles, for 3 particular choices $\phi = 0.01$, $\phi = 0.025$ and $\phi = 0.05$: (*a*) the change in the normalized number of bubbles against rescaled time; (*b*) histogram of the number of ruptures in the first phase of coalescence; (*c*) histogram of the time interval for the first phase of coalescence. Here, the other system parameters are fixed as $P_0 = 1.0$, $h_0 = 0.01$, $S = 10^{-10}$ and $d = 0.1$.

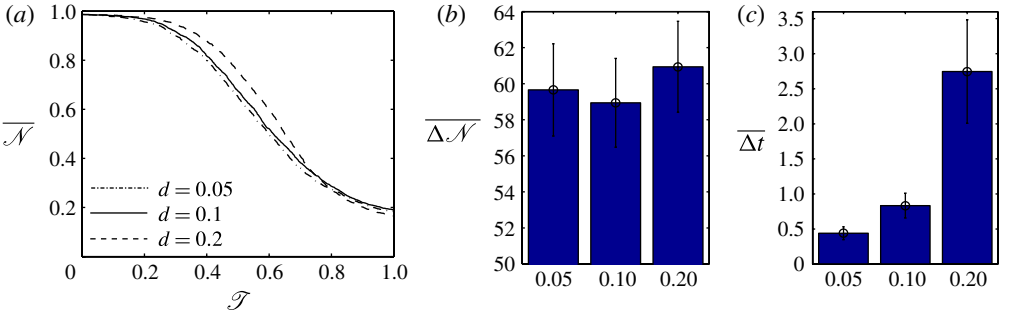

FIGURE 9. (Colour online) The standard deviation of the film thickness for $d = 0.05$, $d = 0.1$ and $d = 0.2$, for a foam initially composed of 72 bubbles: (*a*) the change in the normalized number of bubbles against rescaled time; (*b*) histogram of the number of ruptures in the first phase of coalescence; (*c*) histogram of the time interval for the first phase of coalescence. Here, the other system parameters are fixed as $P_0 = 1.0$, $\phi = 0.05$, $h_0 = 0.01$ and $S = 10^{-10}$.

3.5. *Standard deviation of the initial film thicknesses*

We also examine the dependency on the imposed inhomogeneity in the initial film thickness (sampled according to (3.1)). The change in the normalized number of bubbles, when plotted against rescaled time (3.2), is shown in figure 9(*a*) highlighting that again the evolution is approximately self-similar, with the number of bubbles remaining in the foam at the end of the first phase of coarsening being approximately constant (figure 9*b*). However, as might be expected, the width of the time interval over which this rearrangement occurs becomes greater as the variance of the distribution of film thicknesses increases (figure 9*c*).

3.6. *Master curve for bubble coalescence*

To gain further insight into the master curve of bubble coalescence, we conducted another 144 simulations for periodic foams starting with 72 bubbles fixing $P_0 = 1.0$, $\phi = 0.05$, $d = 0.1$, $S = 10^{-10}$ and $h_0 = 0.01$ to obtain a smoother approximation to the master curve, shown in figure 10(*a*). The stepwise nature of this curve suggests fitting

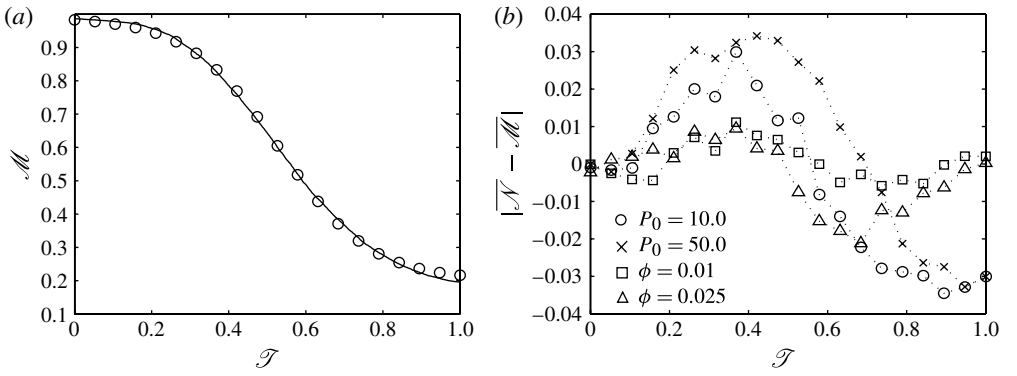

FIGURE 10. Master curve for coalescence in a periodic domain starting from 72 bubbles: (*a*) mean number of bubbles computed from 144 simulations (solid line) plotted against rescaled time; (*b*) absolute error between the master curve and the normalized number of bubbles for other parameter choices with 72 bubbles, sampled at 10 equally spaced points. The fitted curve $\mathscr{M}(\mathscr{T})$ (3.3*a*) is shown as open circles on (*a*).

using a hyperbolic tangent function of $\mathscr{T}$, with three parameters, k, $\mathscr{T}_0$ and $\mathscr{M}_0$ in the form,

$$\mathscr{M}(\mathscr{T}) = \mathscr{M}_0 - \tfrac{1}{2}\overline{\Delta\mathscr{N}}\tanh(k(\mathscr{T} - \mathscr{T}_0)). \tag{3.3a}$$

Least squares fitting of the curve using 20 gridpoints (using `fminsearch` in MATLAB), results in the choice

$$k \approx 4.09608, \quad \mathscr{T}_0 \approx 0.53232, \quad \mathscr{M}_0 \approx 0.59545, \tag{3.3b}$$

with a r.m.s. error of 0.735 %. The fitted curve is shown as open circles on figure 10(*a*). The mean rate of coarsening can then be approximated as a function of the current number of bubbles by taking the derivative of $\mathscr{M}$ with respect to $\mathscr{T}$.

This large number of runs also provides a better estimate of the number of bubbles in the quasi-equilibrium state compared with the initial number, with $\overline{\mathscr{N}}(1) \approx 0.19618$.

For other parameter combinations with 72 bubbles initially (see table 2), we can also estimate the error between the normalized number of bubbles and this master curve, discretizing $\mathscr{T}$ into 20 equally spaced points and computing the absolute error between the two curves at these points, illustrated on figure 10(*b*). We find that the absolute error is bounded by 0.04 in all cases, so this master curve is reasonable approximation to the rescaled data.

However, the rate of bubble coalescence in an individual simulation still depends strongly on the system parameters through the time interval Δt. Assuming a power-law dependency on each of the parameters of interest, we express this in the form

$$\Delta t = f(S, h_0) P_0^{\alpha} \phi^{\beta} d^{\gamma}. \tag{3.4a}$$

The simulations in § 3.2 suggest that $\alpha < 0$, $\beta > 0$ and $\gamma > 0$. The dependency of this time interval on the Sheludko number and initial film thickness has not been considered, and is represented by the functional $f(S, h_0)$. Fitting the coefficients in (3.4*a*) based on the three combinations considered for each parameter of interest

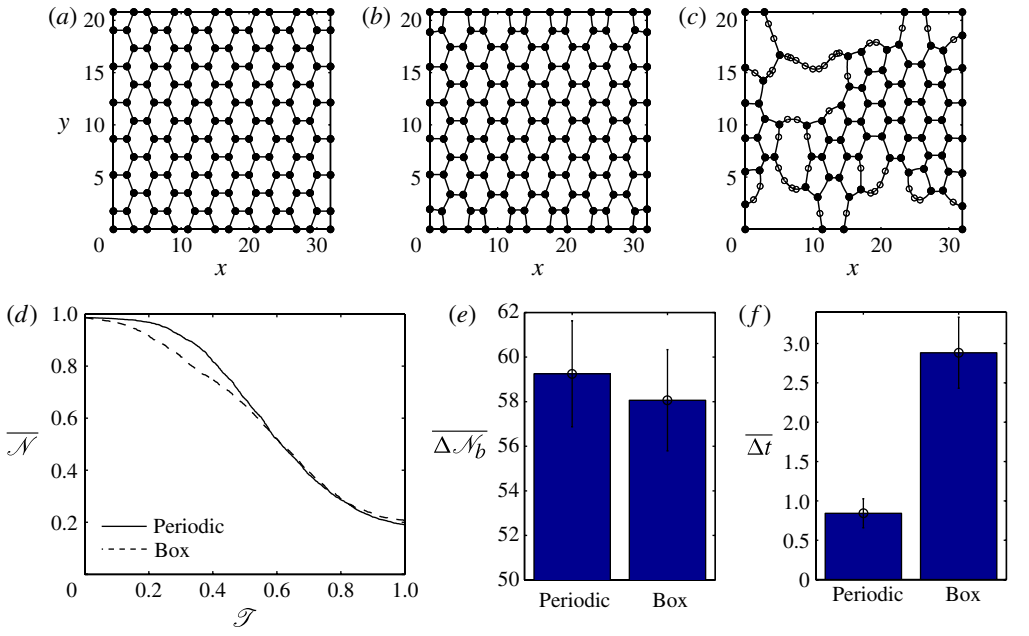

FIGURE 11. (Colour online) Coalescence in a foam initially composed of 72 bubbles confined within a prewetted box: (*a*) initial bubble arrangement; (*b*) bubble arrangement during the static equilibrium phase; (*c*) snapshot of coalescence during the first phase; (*d*) the change in the normalized number of bubbles against rescaled time; (*e*) histogram of the number of ruptures in the first phase of coalescence; (*f*) histogram of the time interval for the first phase of coalescence. Here, the other system parameters are fixed as $P_0 = 1.0$, $\phi = 0.0783$, $h_0 = 0.01$ and $S = 10^{-10}$, $d = 0.1$.

(holding everything else fixed), we calculate

$$\alpha \approx -0.103, \quad \beta \approx 0.285, \quad \gamma \approx 1.321. \tag{3.4b}$$

However, a much larger sweep of parameter space would be required to confirm power-law behaviour and construct these coefficients definitively.

4. Coalescence in a foam confined within a solid box

We can use a similar approach to examine the evolution of a surfactant-free foam evolving within a prewetted solid box. The set-up of this model is described in SD, with further details on how the boundary PBs slide over the liquid lining on the walls; the foam is assigned an initial structure shown in figure 11(*a*), with gas allocated to each bubble to ensure bubbles are equally pressurized to P_0. This configuration is not a static equilibrium (some films do not meet walls tangentially) and the foam evolves over short time scales to the arrangement shown in figure 11(*b*). A typical snapshot of the foam structure at a much later time is given in figure 11(*c*). Several examples of coalescence in a box are given in SD, as well as a movie of the dynamics.

We conduct simulations of the foam illustrated in figure 11(*b*), sampling the initial film thicknesses according to (3.1). For consistency, the films lining the walls of the box must be chosen to be thicker, $h_f \sim a_0^{2/3} h_0^{1/3}$ (further details in SD). We choose a

liquid fraction to ensure C is identical to the case with $\phi = 0.05$ in a periodic domain, and a summary of 32 simulations is given in table 2.

We again normalize the current number of bubbles by the initial number, and rescale time according to (3.2). The corresponding change in the mean number of bubbles (over 32 simulations) is shown in figure 11(*d*), compared with the master curve for evolution in a periodic domain. These two curves compare very well for late times (almost overlapping), but at early times the dynamics in the box appears to be faster, attributed to the bias introduced in the system by the node rearrangement on short time scales, which results in the foam preferentially rupturing films close to the walls. Interestingly, the mean number of bubbles remaining in the system at the end of the first phase of coalescence is almost identical to the periodic foam (figure 11*e*). However, the mean time taken for this phase of rearrangement is now much longer (figure 11*f*), indicating that confinement can significantly reduce the rate of bubble coalescence.

5. Discussion

We have constructed a large-scale network model for the dynamics of a clean liquid foam in a two-dimensional periodic domain, based on an existing formulation for a foam evolving within a prewetted box (Stewart & Davis 2012). This model is essentially a new method for conducting numerical experiments on surfactant-free foams, illuminating time scales not currently accessible to the experimentalist.

Our model has many similarities to the model discussed in Bolton & Weaire (1992) (see also Weaire & Hutzler 1999) for aqueous foams in the dry limit. However, in clean foams (in the absence of surfactant and stabilizing colloidal particles) liquid dynamics must be included explicitly and the foam is never in equilibrium. The model incorporates coupling between pressure and area in the gas bubbles, surface tension on the gas–liquid interfaces, bending and elongational flows in the liquid films and a criterion for film rupture. However, one drawback of this approach is that because all of the area of liquid in a PB is reduced to a single point in space, the estimate of the bubble side length $2(L + a_0)$ becomes increasingly worse as the liquid fraction increases.

We conducted Monte Carlo simulations of our model, showing that after a transient (depending on the initial thickness of the films), the first film rupture triggers a sequence of further breakages and induces a long phase of topological rearrangement. Eventually, the remaining films sweep up sufficient liquid from redundant PBs to restabilize the foam into a new quasi-equilibrium; the mean number of bubbles in this structure (averaged over a large number of simulations) is approximately independent of the system parameters, $\sim$19 % of the initial number. The time interval for this phase of coalescence appears to saturate as the initial number of bubbles becomes large (figure 6*e*), but decreases with the baseline pressure in the bubbles (figure 7*c*) and increases with both the foam liquid fraction (figure 8*c*) and the variance in the distribution of initial film thickness (figure 9*c*); we approximated this parametric dependence by fitting with a simple power law (3.4). In addition, when the time variable is rescaled to normalize the interval of coarsening to the unit interval, we showed that the coalescence is approximately self-similar across a wide area of parameter space (figures 6*b*, 7*a*, 8*a*, 9*a*) and this normalized curve can be well approximated using a hyperbolic tangent function involving only three parameters (3.3*a*). When this time rescaling is applied to simulations of bubble coalescence in foams confined within a prewetted box, the change in the mean number of

bubbles agrees well with the periodic domain (figure 11*e*), although there is a slight discrepancy at early times due to bias introduced by short time scale rearrangement of the nodes in the confined case (figure 11*d*).

Over longer time scales, the bubbles continue to coalesce until the system is composed of only a small number of isolated gas bubbles (so all of the PBs have been absorbed into the films). We expect the dynamics of this coalescence process will be more akin to diffusion-driven coarsening in aqueous foams (Weaire & Hutzler 1999), with the number of bubbles remaining exhibiting a power-law dependency on time for long times. In addition, it would be interesting to consider the dynamics of coalescence in three-dimensional foams or those initiated from a polydisperse state. However, investigation of these questions is deferred to future work.

Acknowledgements

This work is funded by NSF grant no. CMMI-0826703. Enlightening discussions with A. Anderson, L. Brush, M. Davis, P. Grassia, M. Gratton and S. Hilgenfeldt are very gratefully acknowledged. We also acknowledge the very helpful feedback from the anonymous referees on the first draft of this manuscript.

Supplementary movies

Supplementary movies are available at http://dx.doi.org/10.1017/jfm.2013.145.

REFERENCES

ANDERSON, A. M., BRUSH, L. N. & DAVIS, S. H. 2010 Foam mechanics: spontaneous rupture of thinning liquid films with plateau borders. *J. Fluid Mech.* **658**, 63–88.

BANHART, J. 2001 Manufacture, characterisation and application of cellular metals and metal foams. *Prog. Mater. Sci.* **46** (6), 559–632.

BANHART, J., STANZICK, H., HELFEN, L. & BAUMBACH, T. 2001 Metal foam evolution studied by synchrotron radioscopy. *Appl. Phys. Lett.* **78**, 1152–1154.

BOLTON, F. & WEAIRE, D. 1992 The effects of plateau borders in the two-dimensional soap froth. II. General simulation and analysis of rigidity loss transition. *Phil. Mag.* B **65**, 473–487.

BREWARD, C. J. W. & HOWELL, P. D. 2002 The drainage of a foam lamella. *J. Fluid Mech.* **458**, 379–406.

BRUSH, L. N. & DAVIS, S. H. 2005 A new law of thinning in foam dynamics. *J. Fluid Mech.* **534**, 227–236.

BURNETT, G. D., CHAE, J. J., TAM, W. Y., DE ALMEIDA, R. M. C. & TABOR, M. 1995 Structure and dynamics of breaking foams. *Phys. Rev.* E **51** (6), 5788–5796.

CHAE, J. J. & TABOR, M. 1997 Dynamics of foams with and without wall rupture. *Phys. Rev.* E **55** (1), 598–610.

ERNEUX, T. & DAVIS, S. H. 1993 Nonlinear rupture of free films. *Phys. Fluids* **5**, 1117–1121.

GARCIA-MORENO, F., RACK, A., HELFEN, L., BAUMBACH, T., ZABLER, S., BABSCAN, N., BANHART, J., MARTIN, T., PONCHUT, C. & DI MICHIEL, M. 2008 Fast processes in liquid metal foams investigated by high-speed synchrotron X-ray microradioscopy. *Appl. Phys. Lett.* **92**, 134104.

GRATTON, M. B. & WITELSKI, T. P. 2008 Coarsening of unstable thin films subject to gravity. *Phys. Rev.* E **77** (1), 16301.

GRATTON, M. B. & WITELSKI, T. P. 2009 Transient and self-similar dynamics in thin film coarsening. *Physica* D **38**, 2380–2394.

HAMSY, A., PAREDES, R., SONNEVILLE-AUBRUN, O., CABANE, B. & BOTET, R. 1999 Dynamical transition in a model for dry foams. *Phys. Rev. Lett.* **82** (16), 3368–3371.

KERN, N., WEAIRE, D., MARTIN, A., HUTZLER, S. & COX, S. J. 2004 The two-dimensional viscous froth model for foam dynamics. *Phys. Rev.* E **70**, 041411.

VAN LENGERICH, H. B., VOGEL, M. J. & STEEN, P. H. 2010 Coarsening of capillary drops coupled by conduit networks. *Phys. Rev.* E **82** (6), 066312.

OKUZONO, T. & KAWASAKI, K. 1995 Intermittent flow behavior of random foams: a computer experiment on foam rheology. *Phys. Rev.* E **51**, 1246–1253.

STEWART, P. S. & DAVIS, S. H. 2012 Dynamics and stability of metallic foams: network modelling. *J. Rheol.* **56**, 543–574.

VANDEWALLE, N., LENTZ, J. F., DORBOLO, S. & BRISBOIS, F. 2001 Avalanches of popping bubbles in collapsing foams. *Phys. Rev. Lett.* **86**, 179–182.

WEAIRE, D., BOLTON, F., HERDTLE, T. & AREF, H. 1992 The effect of strain upon the topology of a soap froth. *Phil. Mag. Lett.* **66** (6), 293–299.

WEAIRE, D. & HUTZLER, S. 1999 *The Physics of Foams*. Oxford University Press.